IOP Publishing and International Atomic Energy Agency Nuclear Fusion
Nucl. Fusion **52** (2012) 094005 (12pp) doi:10.1088/0029-5515/52/9/094005

Initial measurements of the DIII-D off-axis neutral beams

W.W. Heidbrink[1], M.A. Van Zeeland[2], B.A. Grierson[3], C.M. Muscatello[1], J.M. Park[4], C.C. Petty[2], R. Prater[2] and Y.B. Zhu[1]

[1] University of California, Irvine, CA, USA
[2] General Atomics, San Diego, CA, USA
[3] Princeton Plasma Physics Laboratory, Princeton, NJ, USA
[4] Oak Ridge National Laboratory, Oak Ridge, TN, USA

Received 13 February 2012, accepted for publication 28 March 2012
Published 3 September 2012
Online at stacks.iop.org/NF/52/094005

Abstract
Two of the eight neutral-beam sources on the DIII-D tokamak were modified to allow injection below the midplane. To validate off-axis beam performance, the various beams are injected sequentially into low-power plasmas that are optimized for accurate neutron, neutral–particle, fast-ion D-alpha and fast-ion pressure measurements. As expected, the fast-ion profile is broader with off-axis injection than with on-axis injection. The driven toroidal rotation also broadens with off-axis injection and the central fast-ion density is several times smaller. The number of trapped ions in the core depends sensitively on the pitch of the magnetic field lines. Comparisons with classical predictions agree with the measurements for some diagnostics but are discrepant for others.

(Some figures may appear in colour only in the online journal)

1. Introduction

Neutral-beam injection efficiently delivers power, current, torque and particles to a fusion plasma. Virtually all early experiments [1] injected the neutrals towards the magnetic axis but, in recent years, many devices have explored off-axis neutral-beam injection [2] because it is widely believed that MHD-stable, steady-state operation requires broad current and pressure profiles [3, 4]. Accordingly, off-axis neutral-beam current drive (NBCD) is planned as the primary current drive source in ITER [5].

The DIII-D tokamak is equipped with eight neutral-beam sources housed in four beamlines. Previously, all eight sources injected into the tokamak at the midplane of the vacuum vessel. Prior to the 2011 experimental campaign, a massive hydraulic lift was installed beneath one of the beamlines to allow vertical steering [6]. When the beamline is elevated, the pair of sources in this beamline inject neutrals through the midplane port and below the midplane in the plasma. The experiments reported here sought to confirm that the modified beamline successfully produces a population of off-axis neutral-beam ions and drives off-axis current.

In 2008, prior to embarking on the beamline modification, a set of experiments on DIII-D investigated off-axis injection in small, vertically shifted plasmas [7–9]. The 2011 check-out experiments were patterned after these earlier studies and proceeded in three steps. Initial experiments concentrated on measurements of beam emission [10] in order to determine the beam deposition profile. This work is reported elsewhere [11]. A second set of experiments patterned after [8] utilized specially designed discharges to compare the fast-ion populations produced by the different sources with theoretical predictions. These results are reported here. A third set of experiments patterned after [9] concentrated on accurate NBCD measurements in H-mode plasmas; these results are also reported elsewhere [12]. In addition to these check-out studies, the new off-axis capability was utilized in many other experiments, including exploration of steady-state operational scenarios and studies of the effect of off-axis injection on fast-ion driven instabilities.

The paper begins with a description of the discharges, diagnostics and modelling (section 2). The heart of the paper is in section 3, where data from each of the fast-ion diagnostics are presented. Section 4 discusses possible reasons that some of the data disagree with theory. The conclusion is in section 5.

2. Apparatus

The beam geometry is illustrated in figure 1. The eight available sources inject at six different injection angles. At DIII-D, the eight sources are identified by their toroidal angle of injection and their position within the beam housing (e.g. the left source in the 30° beamline is called '30LT'). In this paper, the sources are labelled by their properties. Six sources

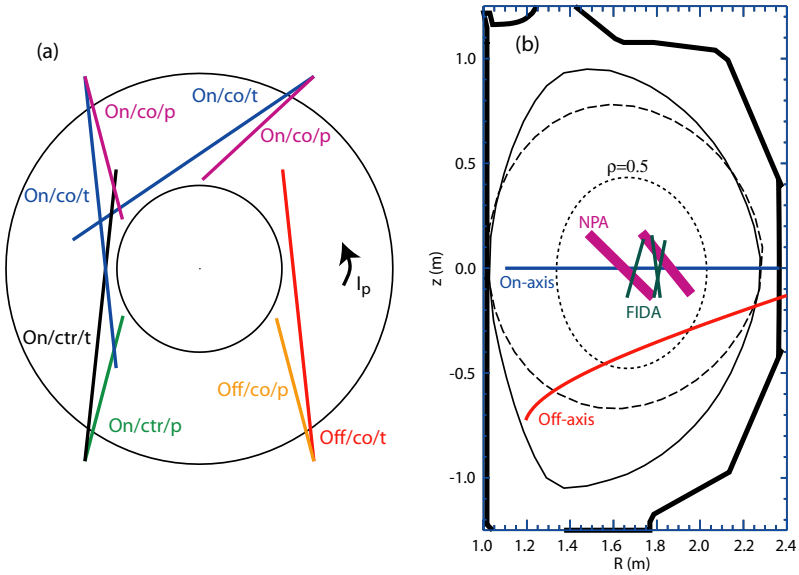

Figure 1. (*a*) Plan view of DIII-D. The lines represent the centre of the various beamlines and are labelled to indicate whether they inject on- or off-axis, in the co- or counter- current direction, and are near-tangential or near-perpendicular toroidally. The plasma current is in the counter-clockwise direction; the toroidal field is either in the clockwise or counter-clockwise direction. (*b*) Elevation of the vacuum vessel, showing projections of the beam centrelines for on- and off-axis injection. The last closed-flux surface (solid line) and half-radius (dotted line) for a typical discharge are shown, as well as the last closed-flux surface (dashed line) for a nearly circular discharge. The lines near the magnetic axis illustrate approximate spatial volumes for the NPA and FIDA measurements shown in figures 11 and 14.

inject in the midplane, while two sources inject downwards at an angle; these differences are called 'On' or 'Off'. Six sources inject toroidally in the direction of the plasma current, while two sources inject toroidally opposite to the plasma current; these differences are called 'co' or 'ctr'. Four sources inject near-tangentially, while four inject more perpendicularly; these differences are called 't' or 'p'. For example, the '30LT' source injects on-axis neutrals in the co-current direction at a near-tangential angle, so it is labelled 'On/co/t' throughout the paper. With the exception of figure 21, the off-axis beams operated at the maximum elevation angle of 16.4° for all of the data in this paper. The plasma current is in the counter-clockwise direction throughout the paper.

A typical plasma shape (figure 1(*b*)) is a diverted discharge with major radius $R_0 \simeq 1.71$ m, minor radius $a \simeq 0.61$ m, elongation $\kappa \simeq 1.8$, and upper (lower) triangularity $\delta \simeq 0.4$ (0.6). To increase the minor radius of off-axis beam injection, a few discharges are nearly circular ($\kappa = 1.1$). The plasma is deuterium, the neutral beams inject deuterium atoms, and the primary impurity is carbon from the graphite walls ($Z_{\rm eff} \simeq 1.5$). The beam voltage (power) is usually 75–81 kV (2.1–2.5 MW). The toroidal field is $B_{\rm T} \simeq 2.0$ T throughout the paper but both clockwise and counter-clockwise directions are employed.

A typical discharge has nearly constant plasma density throughout the discharge (figure 2(*b*)) and is in L-mode. In some cases, the plasma current is constant while, in others, the current ramps up and down in an approximately triangular waveform (figure 2(*a*)). The beams cycle through a repetitive pattern throughout the discharge. Since the plasma conditions are approximately constant, this enables *relative* comparisons of the efficacy of the various sources, eliminating diagnostic calibration errors as a source of uncertainty in the comparisons. In the discharge shown in figure 2, the beams only inject 5% of

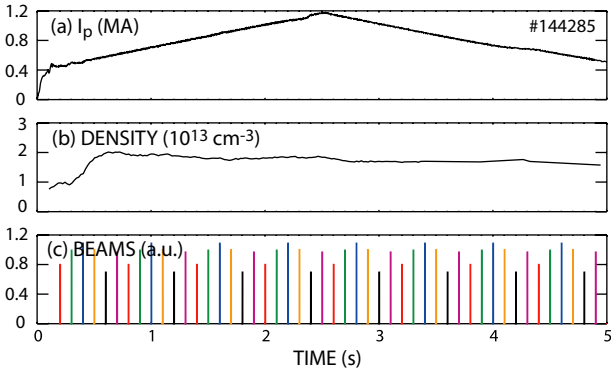

Figure 2. Time evolution of (*a*) plasma current, (*b*) electron density $\bar{n}_{\rm e}$ and (*c*) beam timing waveforms in a discharge optimized for relative measurements of the neutron response to beam blips.

the time, while 2.0 MW of electron cyclotron heating (ECH) is employed throughout the discharge, so the central electron and ion temperatures are $T_{\rm e} = 2.0$ and $T_{\rm i} = 0.9$ keV. In other discharges, the cycling neutral-beam sources steadily inject 2.1–2.5 MW and ECH is not employed, so typical central electron and ion temperatures in those discharges are $T_{\rm i} \simeq T_{\rm e} = 1.7$ keV.

Neutron, fast-ion D-alpha (FIDA) and neutral-particle analyser (NPA) detectors are the primary beam-ion diagnostics. A pair of scintillators measure the volume-averaged neutron rate with good temporal resolution, while a calibrated fission detector provides the absolute calibration with a possible systematic calibration uncertainty of ∼15% [13]. To facilitate comparison of the sources, the neutron calibration is often adjusted within its uncertainty in the figures that follow. Beam-plasma reactions predominate, so the neutron signal is approximately proportional to the number of confined fast ions for these conditions.

Three different instruments measure FIDA light. One instrument has an approximately vertical view [14], so it is more sensitive to trapped ions than to passing ions. A second instrument views the plasma at an oblique angle [15], so it is primarily sensitive to co-passing ions. The approximate spatial resolution of central channels of these two instruments is illustrated in figure 1(*b*). A third instrument, the newly installed main-ion charge-exchange recombination (CER) diagnostic [16], has an essentially tangential view, so its diagnostic sensitivity is strongly weighted towards passing fast ions. Beam modulation of the active beam is used to subtract the background light.

Two solid-state neutral-particle analysers measure escaping neutrals. The signals are measured in current mode, so the relative contribution of different neutrals is approximately proportional to the neutral energy. The analyser sightlines are near-perpendicular, so the measurements are exclusively sensitive to trapped ions. Beam modulation is used to separate the active signal from the passive signal. The approximate spatial resolution of the two active channels is illustrated in figure 1(*b*).

Apart from sawtooth oscillations, the analysed discharges are essentially free of MHD activity. The data presented in section 3 are from all phases of the sawtooth cycle.

The NUBEAM module [17] of the TRANSP code [18] calculates the expected fast-ion distribution function. The first step in TRANSP analysis is calculation of the equilibrium by the EFIT code [19]. In most cases, equilibria are based on magnetics and motional Stark emission (MSE) measurements. The requirement that the electron temperature should be a flux function provides a check on the position of the magnetic axis. Next, kinetic data are mapped onto the equilibrium. The electron density n_e is measured by four interferometers [20], by Thomson scattering [21], and, in some discharges, by profile reflectometry [22]. In the absence of profile reflectometry measurements, the central n_e measurements have large ($\gtrsim$20%) uncertainties. The electron temperature is measured by Thomson scattering and by electron cyclotron emission [23]. The estimated accuracy of these profiles is better than 10%. The CER diagnostic [24] measures the temperature, toroidal rotation and density of carbon ions.

The description of the neutral beams is an important part of the NUBEAM modelling. To match accurately the measured beam-emission profile of the off-axis beams, the power injected by each off-axis source is subdivided into four beamlets. The species mix is assumed constant in time, although spectroscopic measurements of the beam emission with the main-ion CER diagnostic indicates that the actual species mix varies in time. The observed temporal variations are greatest for the half- and third-energy components; since the primary fast-ion diagnostics are most sensitive to the full-energy component, these variations are neglected in the TRANSP modelling. The injected power for each source is based on time-averaged current and voltage waveforms and on calculations of several efficiencies (such as the neutralization efficiency).

The calculated distribution function depends on numerous settings within NUBEAM. Recently, programmed ADAS cross sections [25] are used in the calculation of beam deposition. Comparison of runs with different calculations of the edge neutral density suggest that the edge neutral-density settings are relatively unimportant in these plasmas. The TRANSP option to include additional ad hoc beam-ion diffusion is *not* utilized in this paper.

A complication for the experiment is that many neutral-beam sources play a dual role as both a source of fast ions and as an active beam for diagnostics. As a result, a typical beam-injection pattern consists of one type of source that injects for ~100 ms, followed by short 10 ms pulses of the diagnostic beams. In the TRANSP modelling, the distribution function is averaged over the 10 ms diagnostic-beam pulse and 'dumped' for subsequent analysis. The FIDASIM synthetic diagnostic code [26] then takes the distribution function and computes the expected FIDA and NPA signals. The data are averaged over the same 10 ms time window as the TRANSP calculation.

3. Experimental results

3.1. Neutron beam blips

Analysis of the response of neutron signals to a short beam pulse is a useful way to assess beam-ion confinement [1]. If the duration of the beam 'blip' Δt is short compared with the fast-ion slowing-down time τ_s, the rate of rise of the signal is proportional to the rate that fast ions are produced in the plasma. Comparison of the subsequent decay of the signal with the expected collisional decay permits detection of anomalous losses. For example, in a classic measurement on JT-60U, enhanced ripple losses caused rapid decay of the neutron signal [27].

Quantitatively, the rate of rise of the signal is approximately [28]

$$\dot{I}_n = \dot{N}_b n_d \langle \sigma v \rangle, \tag{1}$$

where $\dot{I}_n$ is the rate of increase in the neutron signal, $\dot{N}_b$ is the rate of increase in the number of confined fast ions, n_d is the deuterium density and $\langle \sigma v \rangle$ is the d–d fusion reactivity. Following the beam blip, if the anomalous losses are negligible, Coulomb collisions cause the signal to decay at a rate that is approximately proportional to the drag on electrons, $\nu_e \propto n_e / T_e^{3/2}$. For cases where the blip duration Δt is not much shorter than τ_s, equation (1) is modified slightly. For all of the data presented here, the fit to the model equations in [28] is excellent.

A typical comparison between theory and experiment appears in figure 3. For this comparison, the experimental absolute calibration has been adjusted to give good agreement with the theoretical prediction for the on-axis beams. (The adjustment is consistent with the absolute calibration of the neutron detectors.) Both the rise and the decay of the signal are in very good agreement with the NUBEAM prediction for the on-axis beams. The shape also agrees fairly well with the expected evolution for the off-axis beam but the magnitude of the initial rise is smaller than predicted.

Figure 4 shows the fits to the neutron waveforms for all of the beam blips in the discharge of figure 2. The rate of rise is a smaller fraction of the predicted rise for the off-axis beams than for the on-axis beams. This implies that these sources produce fewer fast ions than expected. In contrast, the decay rate agrees well with theory for all beam orientations.

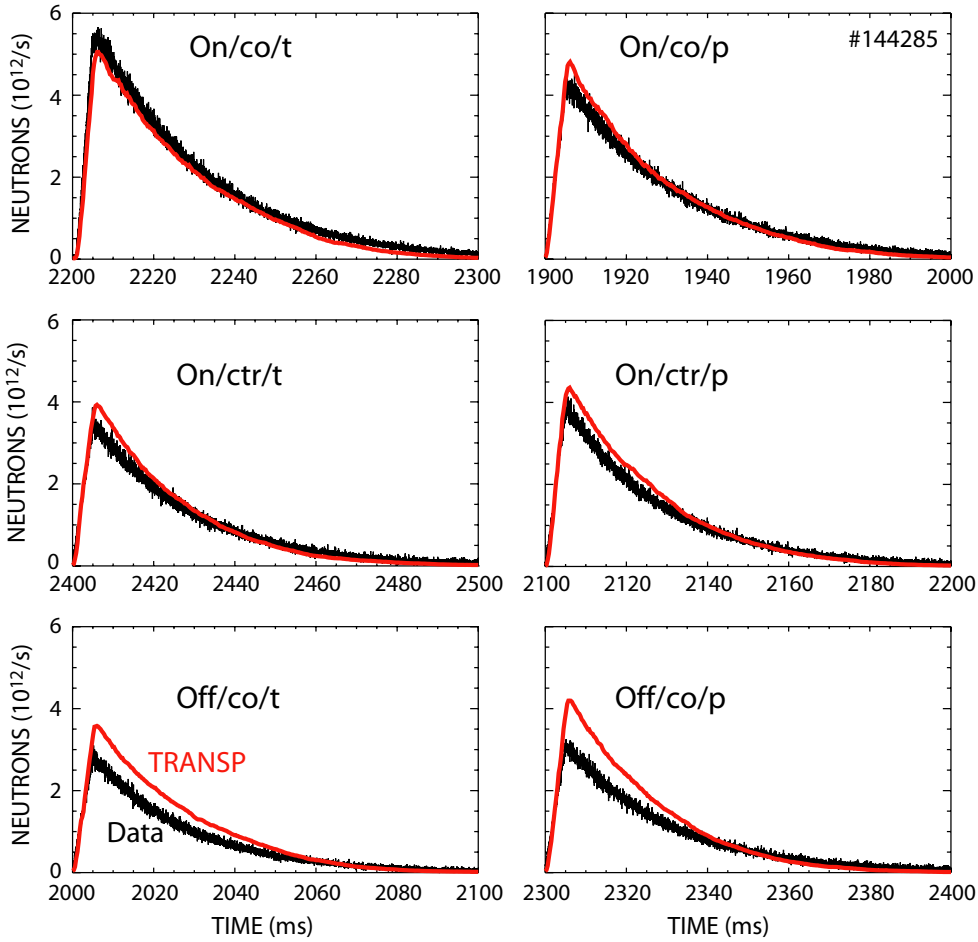

Figure 3. Response of the neutron rate to a 5 ms beam blip from each of the six beam orientations for the discharge shown in figure 2. The smooth curves are the evolution predicted by TRANSP. The experimental calibration has been adjusted within the experimental uncertainty to match the TRANSP predictions for the on-axis co-injected sources. $B_T = +2.0$ T; beam voltages = 54–55 keV.

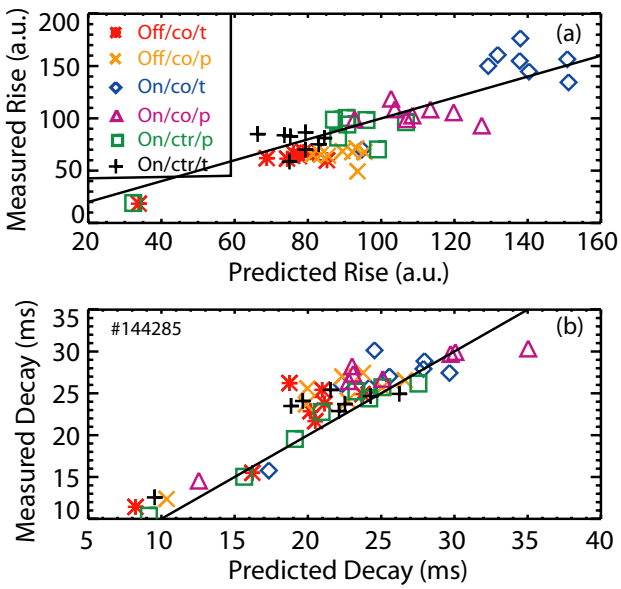

Figure 4. Fits to (*a*) the rate of rise and (*b*) the decay of the neutron signal for the discharge of figure 2. The orientation of the source is indicated by the symbols. The lines show equality between experiment and theory (with a fitted normalization factor in (*a*)).

This implies that the fast ions that are produced by the off-axis beams are confined as well as the fast ions produced by the on-axis beams. The ratio of experiment-to-theory in figure 4 shows no systematic dependence on plasma current, implying that TRANSP correctly models effects associated with the fast-ion banana width.

Beam-blip discharges similar to the one shown in figure 2 were produced several different times during the 2011 campaign and the trends shown in figure 4 are representative. The ratio of off-axis to on-axis rise coefficient is insensitive to the injection energy for values between 45 and 75 keV. Decay rates are similar for all sources. The off-axis rise coefficient is lower than theory for discharges throughout the campaign.

3.2. Single-source neutron data

Another way to use neutron data to assess the beam-ion confinement is to inject each source for longer than a slowing-down time (figure 5). In this case, the neutron signal asymptotically approaches a constant value and the fast-ion distribution function approximates the steady-state value. Beam-plasma reactions predominate, so the neutron rate is proportional to

$$I_n \propto \dot{N}_b n_d \tau_s \propto \dot{N}_b (n_d/n_e) f(T_e). \qquad (2)$$

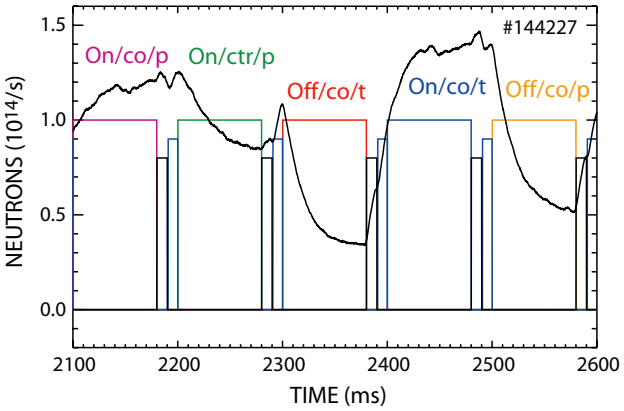

Figure 5. Neutron rate in a discharge with repetitive cycling of beams with five different orientations. After each 80 ms pulse, the On/ctr/t beam is pulsed on for 10 ms for FIDA and NPA measurements and one of the On/co/t beams is pulsed on for 10 ms for CER and MSE measurements. Plasma current as in figure 2; $\bar{n}_e = 3.0 \times 10^{13}$ cm^{-3}; $B_T = +2.0$ T.

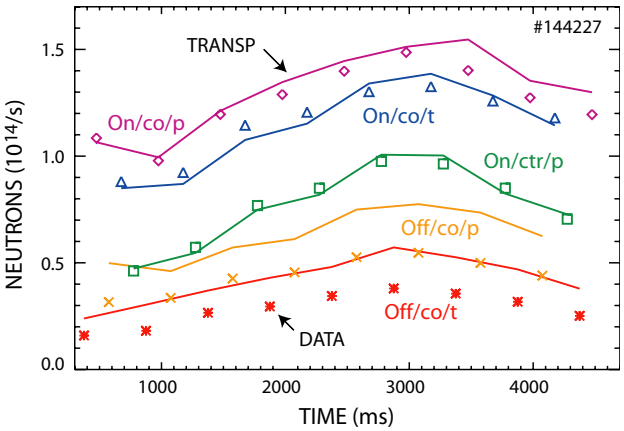

Figure 6. Neutron rate at the end of each 80 ms beam pulse versus time in the discharge shown in figure 5. The data are represented by symbols and the solid lines are the TRANSP predictions. The theoretical prediction has been reduced by 11% to match the on-axis, co-injected data.

Here $f(T_e)$ is a function of the electron temperature that depends on the fast-ion energy relative to the critical energy. (The critical energy is the energy where drag on electrons equals drag on thermal ions.) In contrast to the beam-blip comparison, which depends sensitively on the rather uncertain deuterium density profile, the steady-state rate depends only on the deuterium concentration (n_d/n_e) and on the electron temperature profile, both of which are known more accurately than n_d. (For example, for the time period shown in figure 6, the Z_{eff} profile is virtually constant in space and time, varying only by 8% for minor radii $\leqslant 0.8$.)

To perform the comparison, the neutron rate is measured at the end of each beam pulse for the various injection angles. Figure 6 shows analysed data for a discharge with a triangular plasma current ramp (figure 2(*a*)) and nearly constant electron density. For all five angles of injection, the neutron rate increases with increasing plasma current. The observed increase is consistent with the theoretical prediction and is primarily caused by the increase in T_e. Because the electron temperature profile is peaked in these L-mode plasmas,

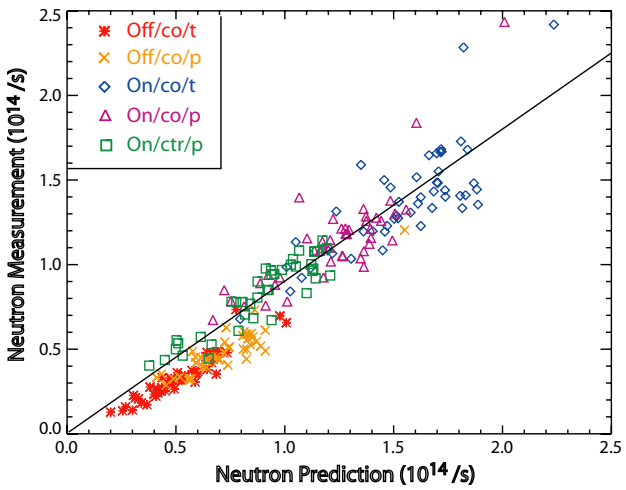

Figure 7. Measured neutron rate at the end of the ~100 ms beam pulse versus predicted neutron rate for eight different discharges. The line shows equality between experiment and theory (with theory multiplied by a normalization factor of 0.9).

theoretically, the on-axis beams are expected to produce more neutrons than the off-axis beams but the difference between on- and off-axis beams is even larger than expected.

Figure 7 shows the ratio of the experimentally observed neutron rate to the theoretically predicted rate for several comparisons of this type. Deficits in the signals relative to the theoretical prediction are consistently observed for both off-axis sources. The deficits occur for both orientations of the toroidal field, for elongated and circular plasmas and for discharges acquired early and late in the 2011 campaign.

3.3. FIDA data

The beam-injection pattern shown in figure 5 is also useful for FIDA measurements of the fast ions. Figure 8 compares spatial profiles at the end of the beam pulse for five different injection angles as measured by three different FIDA diagnostics. The profiles show the expected trends. For the vertically viewing FIDA diagnostic, the signals from the perpendicular beams are larger than from the tangential beams for both on- and off-axis injection. In contrast, the tangentially viewing FIDA diagnostics generally observe larger signals for the tangential sources. As expected, the off-axis beams produce far less signal in the central channels than the on-axis beams.

Figure 9 shows a quantitative comparison between theory and experiment for the vertically viewing FIDA diagnostic. The shapes of the spatial profiles agree qualitatively with theory but the quantitative agreement is only fair. Other analysed discharges show similar levels of agreement for the vertical and oblique FIDA systems. The FIDA signal is proportional to the product of the fast-ion density and the injected neutral density $n_f n_{inj}$. The calculated value of n_{inj} is sensitive to uncertainties in the electron density profile, which can be substantial (especially near the magnetic axis). Experimentally, the profiles depend on the accuracy of the channel-to-channel calibration. An intensity calibration was performed prior to the campaign but subsequent changes in transmission may have occurred.

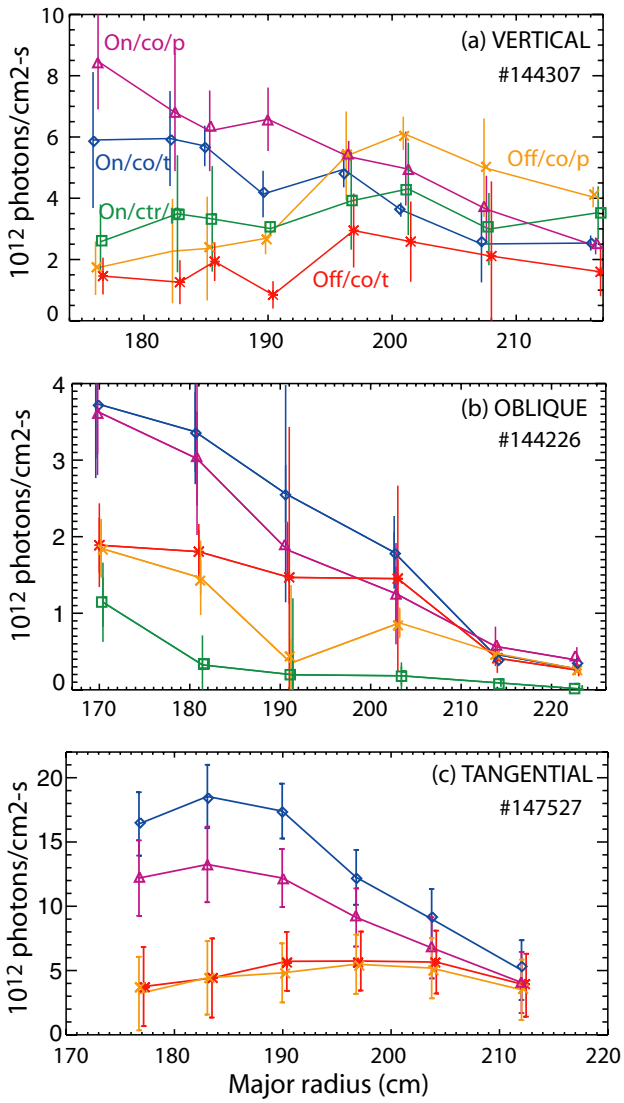

Figure 8. FIDA radial profiles after integration over the blue-shifted FIDA feature at the end of ~100 ms beam pulses for five beam orientations. (*a*) Vertical-viewing diagnostic in a discharge with $B_T = -2.0$ T; wavelength integration from 650.5–652.7 nm. (*b*) Diagnostic with oblique views in a discharge with $B_T = +2.0$ T; wavelength integration from 650.5–652.7 nm. (*c*) Tangentially viewing diagnostic in a discharge with $B_T = -2.0$ T; wavelength integration from 651.0 to 654.0 nm.

The most accurate comparison of the spatial profile with theory was obtained at the end of the campaign with the tangentially viewing main-ion CER diagnostic (figure 10). This diagnostic measures and fits the entire D-alpha spectrum. The FIDA emission is proportional to the product of the injected neutral density n_{inj} and the fast-ion density n_f. Fits to the beam-emission spectra (figures 10(*e*) and (*f*) confirm that the injected neutral density profile of the *diagnostic* beam is approximately stationary in time and is accurately modelled in FIDASIM. The FIDA measurements show that, as expected, the fast-ion profile shifts away from the magnetic axis with off-axis injection (figures 10(*a*)–(*d*)) but the magnitude of the off-axis profile is smaller than expected. Quantitatively, the on-axis signal is ~80% of the predicted value while the off-axis signal is ~60% of the prediction.

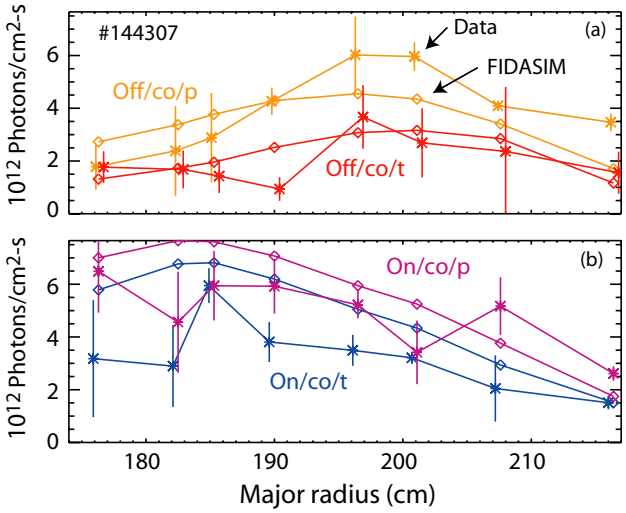

Figure 9. Comparison of the FIDA profiles measured by the vertically viewing system (*) with the prediction of FIDASIM (◇) for (*a*) two off-axis sources and (*b*) two on-axis sources in a discharge with $B_T = -2.0$ T. Wavelength integration from 650.5 to 652.7 nm.

The parametric dependences of the measured FIDA signals are in good agreement with theory. Figure 11 compares measured and predicted signals for central channels from two of the FIDA diagnostics for a number of discharges with different shapes and toroidal-field polarities. A strong correlation between theory and experiment is observed for both systems.

The shape of the FIDA spectra depends on the fast-ion velocity distribution. If Coulomb scattering governs the velocity-space evolution, the measured spectra should agree with theoretical predictions. For the spectra that are summarized in figure 11, the measured spectral shapes are in excellent agreement with theory, with an average reduced $\chi^2_r \lesssim 0.5$ for all angles of injection.

3.4. NPA data

Theoretically, the pitch of the magnetic field line is an important parameter for off-axis neutral-beam injection [7]. If the beam centreline is aligned with the magnetic field line, the parallel velocity component $v_\parallel/v$ is relatively large. Most fast ions execute passing orbits and remain close to the flux surface of their birth. In contrast, for the opposite field polarity, the perpendicular velocity component $v_\perp/v$ is relatively large. For this helicity, many fast ions execute banana orbits that carry them close to the magnetic axis. Figure 12 shows examples of two orbits that ionize at the same position in nominally identical discharges with opposite field helicities. Orbits created by the aligned orientation of the magnetic field are more favourable for NBCD.

Because the NPA diagnostic measures confined fast ions with a well-defined, nearly perpendicular pitch, it is well suited for an investigation of the dependence of the fast-ion distribution function on field helicity. Figure 13 compares two nearly identical discharges that have opposite field helicities. These discharges both have a triangular current ramp, as in figure 2(*a*). The NPA measurements of (predominately)

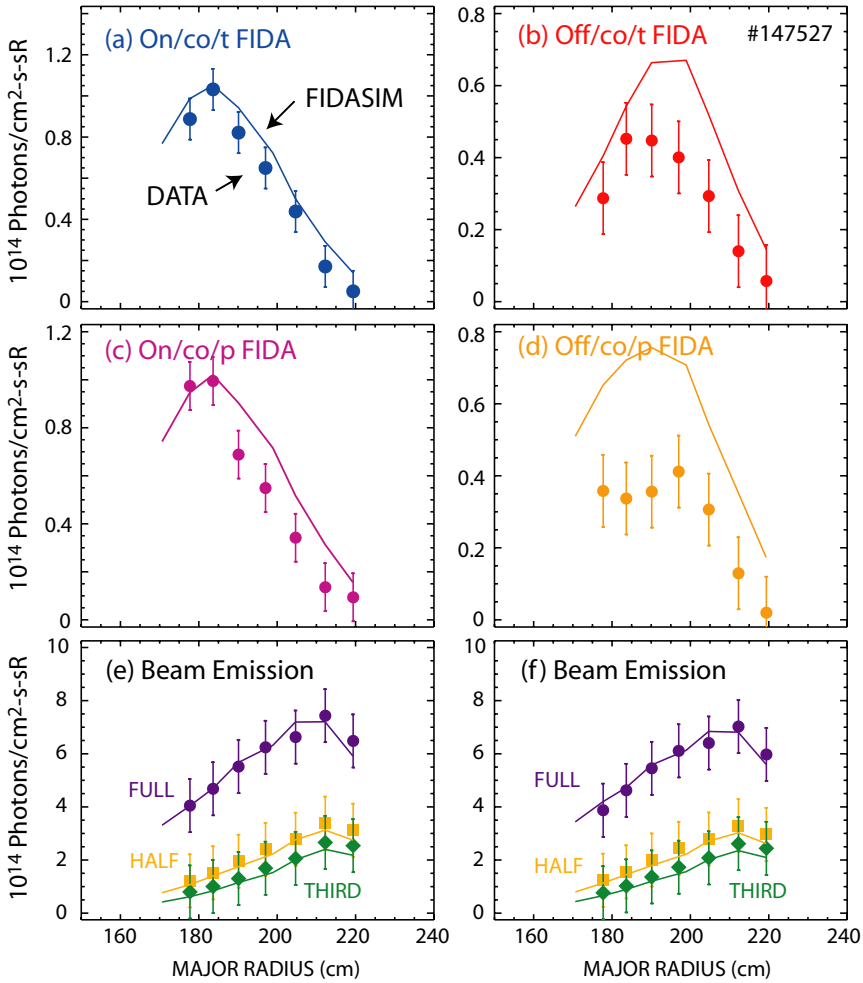

Figure 10. Comparison of the FIDA profiles (symbols) as measured by the tangentially viewing main-ion CER diagnostic with the prediction of FIDASIM (solid lines) for the (*a*) On/co/t, (*b*) Off/co/t, (*c*) On/co/p and (*d*) Off/co/p sources. Measured beam emission from the three beam components at the time of the (*e*) On/co/t and (*f*) Off/co/t measurements. The FIDA brightness is from a fit to the entire feature between 650 and 660 nm. Plasma current as in figure 2; $\bar{n}_e = 2.8 \times 10^{13}$ cm^{-3}; $B_T = -2.0$ T.

trapped particles are in excellent qualitative agreement with theoretical expectations.

- For both on-axis and off-axis injection, the more perpendicular source produces many more trapped ions than the more tangential source.
- For both perpendicular and tangential injection, the on-axis sources produce more on-axis fast ions than the off-axis sources.
- Both on-axis sources are insensitive to the helicity of the field.
- In contrast, both off-axis sources are quite sensitive to field helicity. The unfavourable helicity produces 1.5–2.0 times more central trapped ions than the favourable helicity.

A similar comparison for a central vertically viewing FIDA channel for these two discharges yields a similar result, although the differences are smaller, which is expected since the FIDA measurement is less localized in velocity space than the NPA measurement.

For the same set of discharges as in figures 7 and 11, the measured NPA signals agree reasonably well with the theoretical predictions (figure 14).

3.5. *Toroidal rotation*

The toroidal rotation profile is quite sensitive to the beam-injection angle. Figure 15 shows measurements of the carbon rotation at the end of the beam pulse for each type of source in the same discharge as figure 5. (The carbon rotation profile is close to the deuterium profile in beam-heated L-mode plasmas with modest values of radial electric field [16].) As expected, the co-going on-axis sources produce peaked co-rotating profiles, the off-axis sources produce rotation profiles that are less peaked and the counter on-axis source drives toroidal rotation in the opposite direction. Because the 80 ms beam pulses are comparable to the momentum-confinement time, the profiles in figure 15 are still evolving and are affected to some extent by the preceding source in the pulse train. As a result, the profile for the tangential off-axis source (which follows the counter source) is suppressed from its steady-state value, while the perpendicular off-axis profile (which follows the co on-axis source) is enhanced relative to its ultimate steady-state value.

The TRANSP code is used to assess whether the neutral-beam torque from the off-axis beams is consistent with theoretical expectations. The key assumption in the analysis is

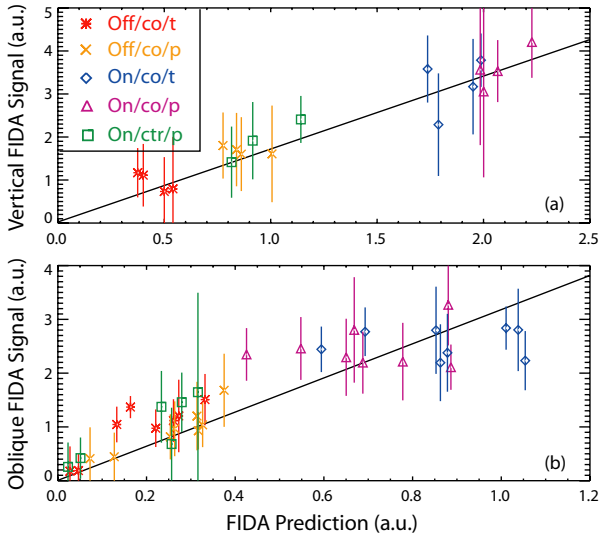

Figure 11. Measured FIDA light versus FIDASIM prediction in five different discharges for (*a*) the vertically viewing channel at $R = 180$ cm and (*b*) the obliquely viewing channels at $R = 170$ cm and $R = 181$ cm. The vertical channel is integrated over 650.8–653.1 nm and the oblique channels are integrated over 650.5–652.7 nm. The lines show agreement between theory and experiment (with an arbitrary normalization factor in each case).

that the momentum diffusivity χ_ϕ of the plasma is independent of neutral-beam source. First, we observe from the initial TRANSP analysis that the thermal-ion diffusivity χ_i hardly changes as the beams cycle through the various angles of injection. Also, the initial analysis shows that the observed momentum diffusivity χ_ϕ is comparable in magnitude to χ_i. Accordingly, we construct a stationary momentum diffusivity profile $\chi_\phi = \langle\chi_i\rangle$, where $\langle\chi_i\rangle$ is temporally averaged over all of the beam pulses. Next, this stationary χ_ϕ profile is used in a predictive TRANSP run in which the rotation profile is free to evolve. If the predicted and measured profiles agree, it indicates that the calculated neutral-beam torque and assumed momentum transport are consistent with the data. Disagreement indicates a deficiency in the torque model or in the momentum-confinement model (or both).

The best available discharge for this analysis is shown in figure 16. In this discharge, the On/co/t diagnostic beam that provides the rotation measurement is on constantly, while the two off-axis sources and two other on-axis sources alternate at 5 Hz. The discharge conditions are nearly constant for five modulation cycles. Figure 16 compares conditionally averaged measured and predicted profiles at various minor radii. As expected, the central rotation decreases with off-axis injection and increases with on-axis injection. At larger radii, only slight variations in rotation speed are observed. The central prediction agrees well with the data but discrepancies are observed at other radii. Overall, the analysis indicates qualitative agreement between theory and experiment. Similar analysis for the discharge shown in figure 15 also shows qualitative but not quantitative agreement between predicted and measured profiles.

3.6. Fast-ion pressure profile

The discharge shown in figure 16 is also well suited for analysis of the fast-ion pressure profile. The On/co/t diagnostic beam that provides the rotation measurement is also the diagnostic beam for the MSE diagnostic. The profile of the total plasma pressure p_{tot} is obtained from EFIT [19] reconstructions of the MHD equilibrium that are consistent with the MSE data, with external magnetics data and with isotherms of the electron temperature. The thermal pressure p_{th} from the T_e, n_e, T_i and carbon density measurements is subtracted from the MHD pressure profile to obtain the fast-ion pressure profile p_f. The difference between the fast-ion pressure produced by on-axis injection and the pressure produced by off-axis injection δp_f is shown in figure 17. Despite large systematic and random errors, it is evident that the profile is more peaked with on-axis injection than with off-axis injection. Although the large uncertainties preclude definite conclusions, the analysis suggests that the difference in pressure is smaller than expected.

3.7. Sawtooth behavior

The response of the sawtooth instability to changes in the angle of injection is qualitatively consistent with the expected change in central power deposition. Figure 18 shows a typical example. The amplitude of the central temperature oscillations ΔT_e is much larger for on-axis injection than for off-axis injection. The changes correlate with calculated changes in central power flow from the beam ions to the electrons. As expected, the Off/co/p beam produces a larger value of ΔT_e than the Off/co/t beam. (The perpendicular off-axis beam produces more trapped ions with orbits that approach the magnetic axis.) Changes in current profile are probably unimportant here. In this discharge, the current diffusion time is much longer than the ~100 ms duration of the different beam pulses and the sawtooth inversion radius (~31 cm wide or about 1/4 of the minor radius) remains virtually constant in time. Counter injection also alters the sawtooth behavior but that is probably due to a change in sawtooth stability [29].

Similar changes in ΔT_e with beam-injection angle are observed for all discharges of this type.

4. Discussion

All available data indicate that the off-axis beams produce a broader fast-ion profile than the on-axis beams. Qualitatively, the off-axis beams have the expected effect on neutron, FIDA, NPA, rotation, pressure, and sawtooth signals.

Table 1 summarizes the results of comparisons with TRANSP NUBEAM calculations for the various diagnostics. In nearly every case, the correlation coefficient r between the experimental data and the theoretical prediction is quite high. This suggests that TRANSP correctly models the parametric dependences of the signals. However, the ratio of theory-to-experiment generally differs for the various sources. (To facilitate comparison, the co-going on-axis values have been adjusted to be nearly unity for all of the diagnostics.) In particular, it appears that the off-axis beams produce fewer fast ions than theoretically predicted. It also seems that the off-axis tangential beam and the counter beam produce a larger fraction of perpendicular ions than predicted by TRANSP.

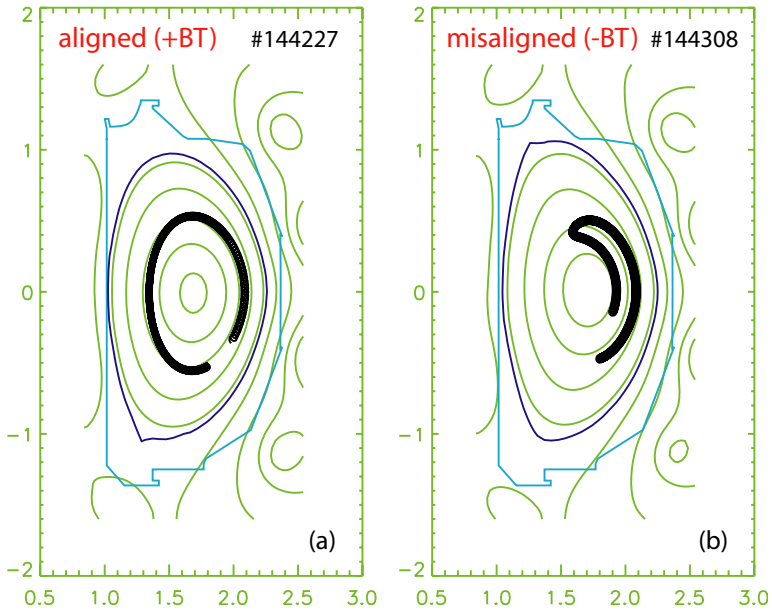

Figure 12. Orbits launched at identical positions along the Off/co/t centreline in experimental equilibria with (*a*) $+B_T$ and (*b*) $-B_T$ field line helicities.

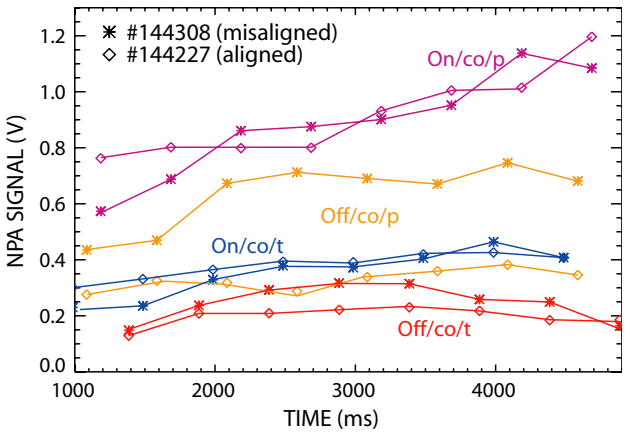

Figure 13. NPA signal at the end of an 80 ms beam pulse for four beam orientations in a pair of nearly identical discharges with $B_T = -2.0$ T (*) and $B_T = +2.0$ T (◇). ($R = 186$ cm NPA channel)

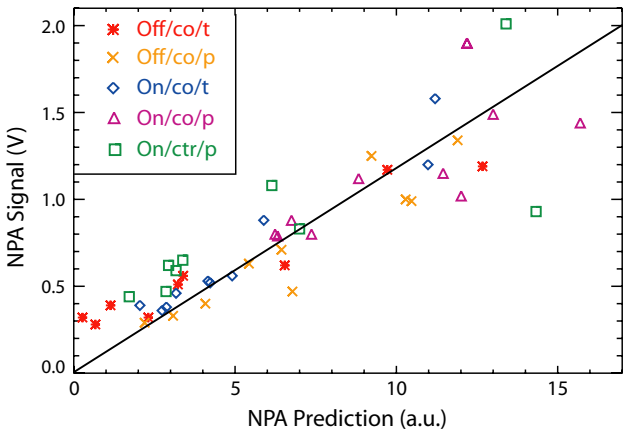

Figure 14. Measured NPA signal versus FIDASIM prediction in five different discharges for the $R = 162$ cm and $R = 186$ cm channels. The line shows equality between theory and experiment (with an arbitrary normalization factor).

Explanations for these discrepancies fall into four categories.

1. *Experimental errors in the fast-ion data.* Because the comparisons consist of relative measurements and there is no evidence of instrumental effects such as detector saturation, this explanation is unlikely.

2. *Uncertainties in plasma profiles and equilibria.* The TRANSP calculations utilize plasma profiles that are mapped onto equilibria generated by EFIT. The beam-blip neutron comparison depends sensitively on the shape of the electron density profile. The FIDA and NPA comparisons are also sensitive to n_e through their underlying dependences on the injected neutral density and on the slowing-down time. In contrast, the steady-state neutron comparison is insensitive to the density profile. Uncertainties in the plasma inputs to TRANSP almost certainly contribute to the observed discrepancies but are unlikely to account for the general observation that the off-axis sources produce less signal than expected.

3. *Inaccuracies in beam modelling.* Great effort was expended to model the geometry of the off-axis beams accurately. Moreover, sensitivity studies with the design beam geometry give very similar neutron predictions as the most careful modelling, so this is an unlikely source of error. On the other hand, other aspects of the beam modelling are likely candidates to explain the discrepancies. Presently, each of the eight DIII-D sources is unique. The operational parameters of each source are individually adjusted to provide reliable performance. Measurements of beam emission show that the species mix evolves in time, particularly for the half- and third-energy components. In the modelling, a temporally constant algorithm computes the species mix for all sources. In addition to uncertainties in species mix, the reported beam power may be inaccurate. The modelling assumes that the

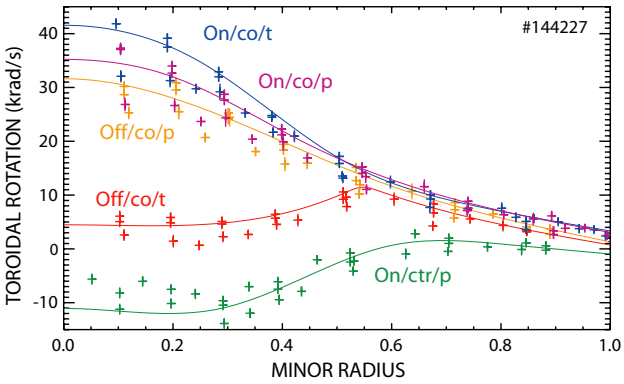

Figure 15. Carbon toroidal rotation profiles at the end of an 80 ms beam pulse for five beam orientations. The curves are spline fits to the measured data (+ symbols). The minor radius is the square root of the normalized toroidal flux.

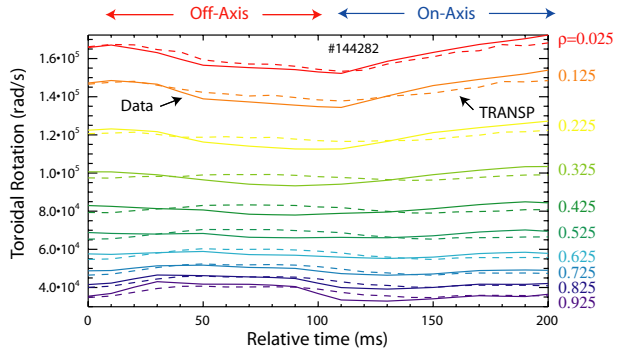

Figure 16. Conditionally averaged toroidal rotation profiles at normalized minor radii between 0.025 and 0.975. One On/co/t beam injects continuously and two off-axis sources and two on-axis sources alternate every 100 ms. The solid curves are the measurements and the dashed curves are the TRANSP predictions for temporally constant momentum transport. $B_T = +2.0$ T; $I_p = 0.9$ MA; $\bar{n}_e = 3.8 \times 10^{13}$ cm^{-3}; H-mode plasma.

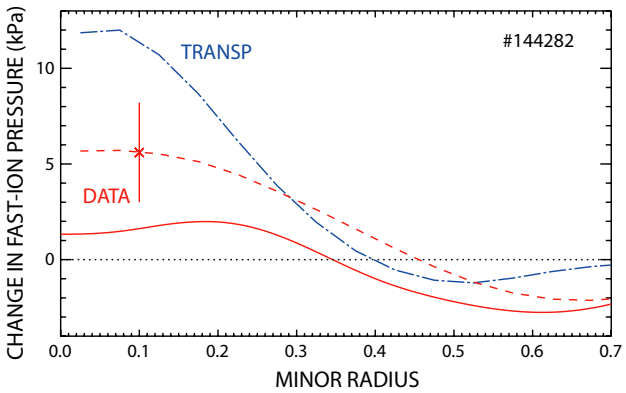

Figure 17. The difference in fast-ion pressure δp_f between on- and off-axis injection for the discharge shown in figure 16. The data are from the end of injection of each type after conditional averaging over five cycles. The solid and dashed lines are from independent equilibrium reconstructions and provide an indication of the magnitude of possible systematic errors; the error bar is an estimate of the random error in determination of the thermal pressure. The dashed–dotted line is the difference in δp_f predicted by TRANSP.

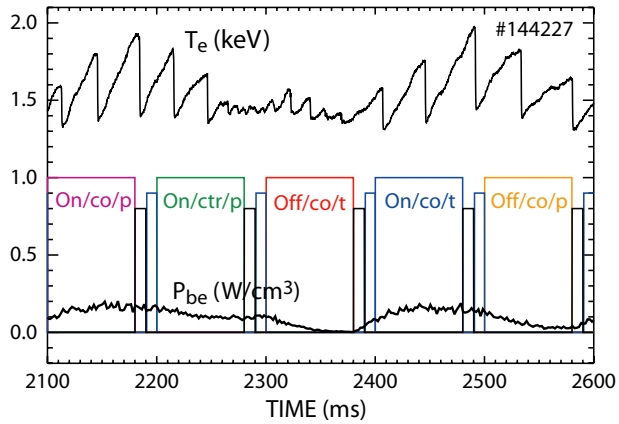

Figure 18. Central electron temperature versus time in the discharge of figure 5. The lower trace shows the on-axis beam power density delivered to electrons as calculated by TRANSP.

power is constant in time but beam-emission measurements suggest there is some temporal variation. In addition, the mean injected power is probably in error. Despite identical injection geometry, neutron beam-blip measurements from the two On/co/t sources can contain discrepancies that exceed the measurement errors (not shown).

4. *Deficiencies in the TRANSP model.* All previous TRANSP modelling in this paper neglects fast-ion transport by instabilities. In reality, transport by sawteeth and by microturbulence will modify the distribution function from the one computed by TRANSP. To investigate the possible effect of these instabilities, new TRANSP simulations are performed. TRANSP can model a Kadomtsev redistribution of fast ions at the sawtooth crash. Recent measurements show that the TRANSP model underestimates the actual redistribution [30]; nevertheless, the TRANSP modelling is useful for a quantitative estimate of the importance of the effect. Because the $q = 1$ radius is modest in these plasmas, the calculated redistribution only occurs in the central quarter of the plasma and has a negligible effect on the calculated volume-averaged neutron rate (figure 19(*a*)). As expected, the reduction is slightly greater for on-axis injection than for off-axis injection but is very small for all angles of injection. On the other hand, the calculated effect on fast-ion profiles is significant. Figure 19(*b*) shows that sawteeth can alter the calculated central fast-ion density $n_f(0)$ by as much as ∼50%. (The changes are smaller at other radii.) This effect may explain why the FIDA profiles in figures 10(*b*) and (*d*) are less hollow than predicted. Similar conclusions apply to the possible transport by microturbulence. Figure 19(*c*) shows TRANSP simulations that include spatially uniform *ad hoc* fast-ion diffusion. Because the fast-ion profile is more peaked for on-axis injection than for off-axis injection, the inclusion of diffusion has a bigger effect on the calculated profile and, consequently, has a larger effect on the calculated neutron rate. Thus, by reducing the theoretical on-axis prediction, the inclusion of spatially uniform diffusion *exacerbates* the neutron discrepancy between theory and experiment. Of course, the actual diffusion is probably larger off-axis than on-axis, so the true effect of diffusion is probably smaller than shown in figure 19(*c*). On the other hand, in earlier DIII-D experiments [31], appreciable discrepancies in neutron and FIDA signals occurred at a significantly higher value of temperature ($T_i \gtrsim 4$ keV) than obtained in the present

Table 1. Experiment-to-theory ratio and correlation coefficient for each beam orientation as measured by four fast-ion diagnostics. The data are from analysis of ∼100 ms beam pulses in 5–8 discharges with $I_p = 0.4$–1.2 MA and $B_T = \pm 2.0$ T.

	Neutron		Vertical FIDA		Oblique FIDA		NPA	
Beam	ratio	r	ratio	r	ratio	r	ratio	r
Off/co/t	0.72 ± 0.10	0.94	0.87 ± 0.34	−0.94	0.62 ± 0.37	0.91	2.4 ± 2.8	0.96
Off/co/p	0.76 ± 0.09	0.91	0.88 ± 0.14	−0.78	0.87 ± 0.49	0.94	0.86 ± 0.15	0.93
On/co/t	1.01 ± 0.13	0.83	1.02 ± 0.22	0.37	1.08 ± 0.65	0.90	1.09 ± 0.18	0.97
On/co/p	1.05 ± 0.11	0.83	0.98 ± 0.09	0.87	0.94 ± 0.58	0.89	0.93 ± 0.17	0.77
On/ctr/p	1.05 ± 0.11	0.92	0.86 ± 0.10	0.98	0.48 ± 0.32	0.99	1.35 ± 0.44	0.78
Overall	—	0.95	—	0.95	—	0.88	—	0.88

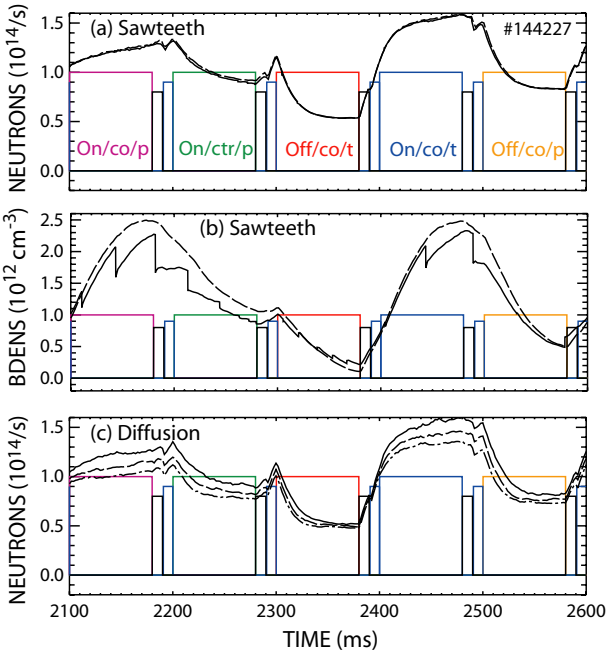

Figure 19. Calculations by TRANSP for various models in the discharge of figure 5. (*a*) Neutron rate with (solid) and without (dashed) Kadomtsev redistribution of fast ions at sawtooth crashes. (*b*) Central fast-ion density with (solid) and without (dashed) Kadomtsev redistribution at sawtooth crashes. (*c*) Neutron rate with spatially uniform fast-ion diffusion of 0 (solid), 0.5 (dashed) and 1.0 m^2 s^{-1} (dashed–dotted).

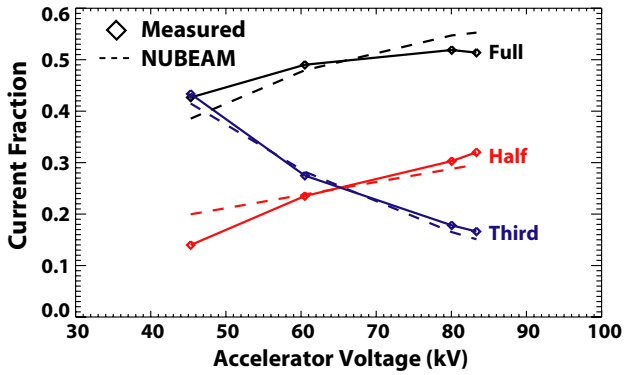

Figure 20. Measured dependence of beam species mix on accelerator voltage for the Off/co/p source (solid lines). The dashed lines show the values employed in NUBEAM modelling in this paper. The actual species mix varies in time; these data are averages that begin 25 ms after the start of injection.

experiment, so large redistribution due to microturbulence seems unlikely here. We conclude that transport by sawteeth and microturbulence probably plays a role in flattening the FIDA profile but is unlikely to account for the neutron discrepancy.

To test the hypothesis that errors in off-axis beam parameters are responsible for the neutron deficit, two special experiments were conducted at the end of the 2011 campaign. The first experiment investigated the species mix. Spectroscopic measurements of beam emission were obtained when the torus was filled with gas and the beams injected for 50 ms. The analysis employs the method described in [32] and will be described in more detail in a forthcoming paper. Figure 20 compares the data with the customary values of species mix employed in the NUBEAM analysis. For most of the data in this paper, the off-axis beams operated at ∼75 keV. The differences between the measured and modelled full-energy component is only a few per cent at this voltage, so error in the species mix can only account for a small percentage of the neutron discrepancy.

The second experiment began by reproducing the beam-blip and single-source discharges with the beamline elevated at 16.4° as before. Next, the 'off-axis' beamline was leveled to inject in the midplane and the two discharges were reproduced. Figure 21(*a*) shows the neutron data when the 'off-axis' beams inject at 0°. The measured neutron rate is substantially lower than predicted by TRANSP, as it is for true off-axis injection. Similarly, the neutron rise in the 0° beam-blip discharge is lower than theoretically predicted. Quantitatively, the neutron rate for the 'Off/co/t' source is 74% of the prediction for the beam pulses in this discharge, while the rate for the 'Off/co/p' source is 91% of the prediction. Figure 21(*b*) compares measured FIDA profiles for two permanently on-axis beams and for two 'off-axis' beams that inject on-axis. Relative to the reported power, the average FIDA brightness for the 'off-axis' beams is ∼75% of the brightness for the permanently on-axis beams. For comparisons of each source individually (not shown), the 'Off/co/t' beam is 87% of the On/co/t beam, while the 'Off/co/p' beam is 70% of the On/co/p beam.

In conclusion, transport by instabilities and errors in profile fitting and species mix are all likely contributors to the observed discrepancies but the major contributor is probably an error in beam power. We note that neutron discrepancies of $\lesssim 20\%$ between sources were also observed in our earlier study of off-axis injection in vertically shifted plasmas [8].

5. Conclusion

All available measurements indicate that the fast-ion profile is broader with off-axis injection than with on-axis injection. The vertically elevated sources are a valuable tool for the study

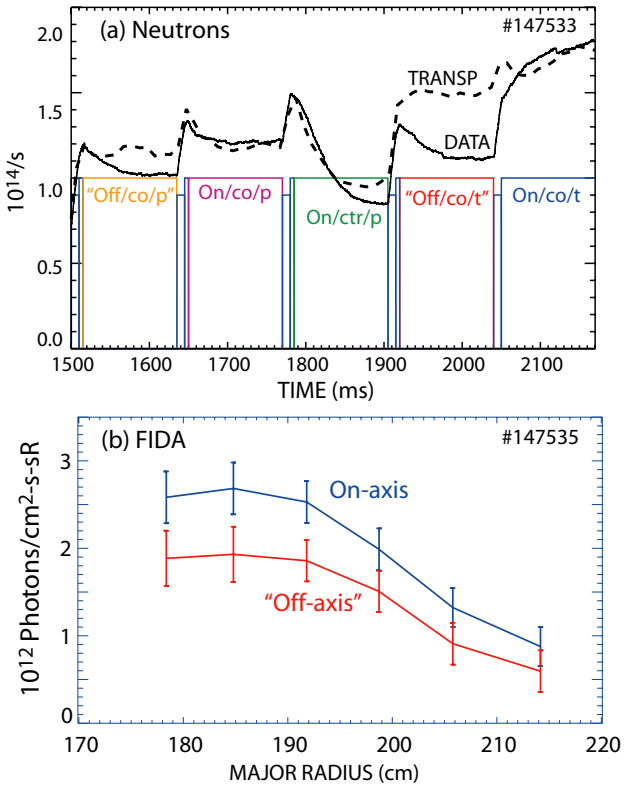

Figure 21. (*a*) Measured (solid) and predicted (dashed) neutron rate for a discharge where all sources inject at the midplane. $B_T = -2.0$ T; triangular plasma current waveform; $\bar{n}_e = 2.3 \times 10^{13}$ cm^{-3}. The predicted rate has been adjusted 10% to match the sources that always inject on-axis. (*b*) FIDA profiles when the two 'Off-axis' sources inject at the midplane and two permanently on-axis sources inject. The data are acquired by the tangentially viewing main-ion CER diagnostic at the end of 100 ms beam pulses. Wavelength integration from 651 to 654 nm; average of four pulses.

of profile effects on plasma stability and confinement. For experiments that require off-axis NBCD, the favourable field helicity should be employed.

The off-axis sources produce ~20% fewer fast ions than expected, probably because the beam power is lower than reported. In future studies, more accurate calorimetry of the beam power for all sources is highly desirable.

Acknowledgments

Our debt to the neutral-beam group for their tremendous efforts in reorienting and operating the elevated beam is gratefully acknowledged, as well as the valuable contributions of other members of the DIII-D team and helpful suggestions by W.M. Solomon. This work was funded by the US Department of Energy under SC-G903402 and DE-FC02-04ER54698, DE-AC02-09CH11466 and DE-AC05-0000R22725.

References

[1] Heidbrink W.W. and Sadler G.J. 1994 *Nucl. Fusion* **34** 535
[2] Suzuki T. *et al* 2011 *Nucl. Fusion* **51** 083020
[3] Turnbull A.D., Taylor T.S., Lin-Liu Y.R. and St. John H. 1995 *Phys. Rev. Lett.* **74** 718
[4] Luce T.C. 2011 *Phys. Plasma* **18** 030501
[5] ITER Physics Expert Group on Energetic Particles, Heating, and Current Drive *et al* 1999 *Nucl. Fusion* **39** 2495
[6] Murphy C. *et al* 2011 Overview of DIII-D off-axis neutral beam project *SOFE: Proc. of the 24th Symp. on Fusion Engineering (Chicago, IL, 2011)* doi:10.1109/SOFE.2011.6052323
[7] Murakami M. *et al* 2009 *Nucl. Fusion* **49** 065031
[8] Heidbrink W.W. *et al* 2009 *Plasma Phys. Control. Fusion* **51** 125001
[9] Park J.M. *et al* 2009 *Phys. Plasma* **16** 092508
[10] Van Zeeland M.A. *et al* 2010 *Plasma Phys. Control. Fusion* **52** 045006
[11] Van Zeeland M.A. *et al* 2011 *Bull. Am. Phys. Soc.* **56** 96
[12] Park J.M. *et al* 2011 *Bull. Am. Phys. Soc.* **56** 96
[13] Heidbrink W.W., Taylor P.L. and Phillips J.A. 1997 *Rev. Sci. Instrum.* **68** 536
[14] Luo Y., Heidbrink W.W., Burrell K.H., Gohil P. and Kaplan D. 2007 *Rev. Sci. Instrum.* **78** 033505
[15] Muscatello C.M., Heidbrink W.W., Taussig D. and Burrell K.H. 2010 *Rev. Sci. Instrum.* **81** 10D316
[16] Grierson B.A., Burrell K.H., Heidbrink W.W., Pablant N.A. and Solomon W.M. 2012 *Phys. Plasma* **19** 056107
[17] Pankin A., Mccune D., Andre R., Bateman G. and Kritz A. 2004 *Comput. Phys. Commun.* **159** 157
[18] Budny R.V. 1994 *Nucl. Fusion* **34** 1247
[19] Lao L.L., St. John H., Stambaugh R.D., Kellman A.G. and Pfeiffer W. 1985 *Nucl. Fusion* **25** 1611
[20] Carlstrom T.N., Ahlgren D.R. and Crosbie J. 1998 *Rev. Sci. Instrum.* **59** 1063
[21] Carlstrom T.N. *et al* 1992 *Rev. Sci. Instrum.* **63** 4901
[22] Zeng L. *et al* 2006 *Nucl. Fusion* **46** S677
[23] Austin M.E. and Lohr J. 2003 *Rev. Sci. Instrum.* **74** 1457
[24] Gohil P., Burrell K.H., Groebner R.J. and Seraydarian R.P. 1990 *Rev. Sci. Instrum.* **61** 2949
[25] Anderson H. *et al* 2000 *Plasma Phys. Control. Fusion* **42** 781
[26] Heidbrink W.W., Liu D., Luo Y., Ruskov E. and Geiger B. 2011 *Commun. Comput. Phys.* **10** 716
[27] Tobita K., Tani K., Nishitani T., Nagashima K. and Kusama Y. 1994 *Nucl. Fusion* **34** 1097
[28] Heidbrink W.W. *et al* 2003 *Nucl. Fusion* **43** 883
[29] Chapman I.T. *et al* 2009 *Nucl. Fusion* **49** 035006
[30] Muscatello C.M. *et al* 2012 *Plasma Phys. Control. Fusion* **54** 025006
[31] Heidbrink W.W., Murakami M., Park J.M., Petty C. C. and Van Zeeland M.A. 2009 *Phys. Rev. Lett.* **103** 175001
[32] Burrell C.F., Cooper W.S., Smith R.R. and Steele W.F. 1980 *Rev. Sci. Instrum.* **51** 1451